Identification of Active Sites for CO_2 Reduction on Graphene-Supported Single-Atom Catalysts

Youngho Kang,*[a] Sungwoo Kang,[b] and Seungwu Han[b]

Transition metal- and nitrogen-codoped graphene (referred to as M–N–G, where M is a transition metal) has emerged as an important type of single-atom catalysts with high selectivities and activities for electrochemical CO_2 reduction (CO_2R) to CO. However, despite extensive previous studies on the catalytic origin, the active site in M–N–G catalysts remains puzzling. In this study, density functional theory calculations and computational hydrogen electrode model is used to investigate CO_2R reaction energies on Zn–N–G, which exhibits outstanding catalytic performance, and to examine kinetic barriers of reduction reactions by using the climbing image nudged elastic band method. We find that single Zn atoms binding to N and C atoms in divacancy sites of graphene cannot serve as active sites to enable CO production, owing to *OCHO formation (* denotes an adsorbate) at an initial protonation process. This contradicts the widely accepted CO_2R mechanism whereby single metal atoms are considered catalytic sites. In contrast, the C atom that is the nearest neighbor of the single Zn atom (C_{NN}) is found to be highly active and the Zn atom plays a role as an enhancer of the catalytic activity of the C_{NN}. Detailed analysis of the CO_2R pathway to CO on the C_{NN} site reveals that *COOH is favorably formed at an initial electrochemical step, and every reaction step becomes downhill in energy at small applied potentials of about −0.3 V with respect to reversible hydrogen electrode. Electronic structure analysis is also used to elucidate the origin of the CO_2R activity of the C_{NN} site.

Introduction

Converting CO_2 into valuable fuels and chemicals helps mitigate the ever-increasing energy crisis as well as global warming. Unfortunately, CO_2 is a fully oxidized chemical species and so thermodynamically stable. As a result, the CO_2 reduction (CO_2R) process is significantly sluggish. To overcome the slow kinetics, diverse transition metals such as Cu, Zn, Au, and Pd have been extensively investigated as heterogeneous electrochemical catalysts for CO_2R, demonstrating meaningful chemical activities.[1–8] For example, CO_2 is converted into various species such as CO, HCOOH, and CH_4 on Cu, whereas CO is primarily produced on Au. However, these catalysts require substantial overpotentials [< -0.8 V vs. reversible hydrogen electrode (RHE)] to drive CO_2R reactions at appreciable rates.

Besides transition metals, a variety of materials such as transition metal dichalcogenides,[9–11] nickel sulfides,[12] and single-atom-doped carbons[13–25] are attracting recent attentions as potential heterogeneous catalysts, especially for CO_2R. In particular, transition metal- and nitrogen-codoped graphene (referred to as M–N–G, where M is a transition metal) has emerged as an important type of single-atom CO_2R catalysts that produce CO with a remarkable activity and efficiency. For example, Ju et al. discovered that M–N–G catalysts (M=Mn, Fe, Co, Ni, and Cu) selectively converts CO_2 into CO with small onset potentials (> -0.3 V vs. RHE) and high faradaic efficiencies (FEs; $>60\%$ in the case of M=Fe and Ni).[20] Yang et al.[16] and Chen et al.[18] independently explored CO_2R reactions on Zn–N–G catalysts and achieved small external potentials in reducing CO_2 to CO; CO starts to be produced above −0.2 V vs. RHE. In addition, Zn–N–G catalysts were found to be exceptionally efficient, showing FEs over 90% for CO production at about −0.4 V vs. RHE. High durability is another advantage of M–N–G catalysts as shown in experimental finding that initial FEs of M–N–G catalysts are maintained after tens of hours of continuous operations.[16,21]

Despite the promising results on M–N–G catalysts, the active site for CO_2R remains elusive, which hampers further optimization of the catalysts. Several groups carried out computational analysis to reveal the catalytic mechanism of M–N–G catalysts.[14,16,19,20] These studies assumed a single metal atom that is embedded at a divacancy site of graphene serves as catalytic sites. However, it turned out that the initial reduction of CO_2 to *COOH (* indicates a pure active site or an adsorbate), which is a key intermediate in the CO production, is energetically unfavorable; the reaction free energy of $* + CO_2 + H^+ + e^- \rightarrow$*COOH was computed to be 1.6 eV and 1.2 eV in Ni–N–G and Zn–N–G catalysts, respectively.[19,20] Furthermore, although most of previous studies assumed *COOH as an initial intermediate, *OCHO may compete with or be more stable than *COOH. Indeed, Han et al. investigated CO_2R on the Zn atom site in the Zn–N–G catalyst and showed that *OCHO, which would lead to the pathway to CH_4 rather than CO, is much lower in energy than *COOH.[19] All these previous results challenge the widely accepted CO_2R mechanism wherein CO_2R reactions proceed on single-metal-atom sites.

[a] Prof. Y. Kang
Department of Materials Science and Engineering
Incheon National University, Incheon 22012 (Republic of Korea)
E-mail: youngho84@inu.ac.kr
[b] S. Kang, Prof. Dr. S. Han
Department of Materials Science and Engineering and Research Institute of Advanced Materials
Seoul National University, Seoul 08826 (Republic of Korea)

Supporting information for this article is available on the WWW under https://doi.org/10.1002/cssc.202100757

In this work, to identify the active site for CO_2R to CO in M–N–G catalysts, we investigate the electrochemical reaction pathways using density functional theory (DFT) calculations and computational hydrogen electrode (CHE) model. We focus on the Zn–N–G catalyst that outperforms other M–N–G catalysts and assume that single Zn atoms are embedded at divacancy sites of graphene, binding to four neighboring N or C atoms, as suggested by previous experiments (Figure 1).[14,18,20,26–28] Our calculations predict that *OCHO is a favorable initial intermediate of CO_2R on the Zn site, indicating that CO cannot be produced on this site. Instead, we find that the C atom that is a chemically-bonded nearest neighbor of the Zn atom (C_{NN}) is highly active for CO_2 reduction to CO, and Zn plays a role as an enhancer of the catalytic activity of the C_{NN}. Detailed analysis on the CO_2R pathways to CO on the C_{NN} site reveals that *COOH is favorably formed at the initial reduction step, and every reaction step becomes downhill in energy at small biases of about −0.3 V vs. RHE. To enlighten the origin of the CO_2R activity of the C_{NN} site, we also analyze electronic structures of the catalysts with and without adsorbates.

Results and Discussion

Figure 1 shows the coordination structures of a single Zn atom adopted for investigating CO_2R reactions. In experiments, N-rich environments around single metal atoms have been reported more frequently in M–N–G catalysts. Indeed, N-decorated divacancies significantly stabilize the single Zn atom, as evidenced by the large binding energies (see the Supporting Information, Figure S1). Nonetheless, the number of M–C and M–N bonds can fluctuate at each M-atom site.[14,18,26] To consider this, we take into account two different configurations: ZnN_4 (Figure 1a) and ZnN_3C (Figure 1b).

The initial reduction of CO_2 can yield either *COOH or *OCHO. The former binds to an active site through C while the latter binds through O. Between these adsorbates, *COOH can lead to CO production via a reaction of $*COOH + H^+ + e^- \rightarrow * + CO + H_2O$. In contrast, *OCHO may open CO_2R pathways to other products like CH_4, but not CO.[19] Because the type of the final reduction product depends on the initial adsorbate, it is important to identify the most stable initial adsorbate. To this end, we compare the reaction free energies ($\triangle G$) of the *COOH and *OCHO formation.

We first examine the possibility that the Zn atom is the active site. The optimized atomic structures of *OCHO and *COOH in a ZnN_4 moiety are shown in Figures 2a and 2b, respectively. In a ZnN_3C moiety, the atomic configurations of the adsorbates are almost the same as those in the ZnN_4 moiety. As shown in Figure 2c, *OCHO is 0.74 eV lower in energy than *COOH in the ZnN_4 moiety, consistent with a previous work.[19] The higher stability of *OCHO is also found in the ZnN_3C moiety; the free-energy difference between *OCHO and *COOH slightly increases to 0.89 eV (Figure 2d). These results manifest that the Zn site cannot be active centers enabling CO production, regardless of the coordination environments.

Next, we calculate $\triangle G$ for the electrochemical reduction of CO_2 to *COOH and *OCHO on the C_{NN} site in a ZnN_3C moiety (the C_{NN} atom is marked with a red dashed circle in Figure 1b). Figures 3a and 3b show the optimized atomic structures of *COOH. We find that the formation of *COOH is exergonic at 0 V vs. RHE, giving rise to $\triangle G$ of −0.16 eV. Thus, the formation of *COOH is thermodynamically favorable. At variance with *COOH, we find no stable configurations for *OCHO, implying *OCHO cannot be formed on the C_{NN} site.

With *COOH as an initial intermediate, we construct the free-energy diagram of the CO_2R pathway to CO (Figure 3c). In this diagram, we consider gaseous CO to be a final product because CO adsorption is energetically undesirable at small negative potentials; $\triangle G$ of $*COOH + H^+ + e^- \rightarrow *CO + H_2O$ is

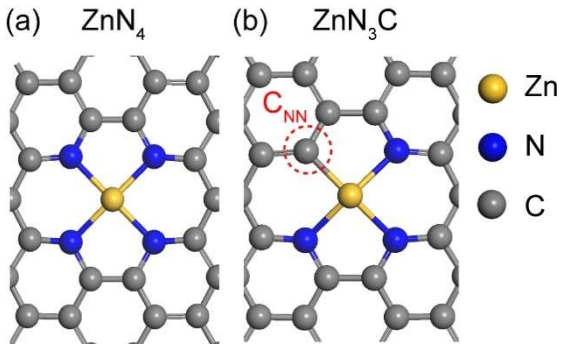

Figure 1. Coordination structures of a single Zn atom in (a) ZnN_4 and (b) ZnN_3C. The C_{NN} atom in ZnN_3C is marked with a red dashed circle.

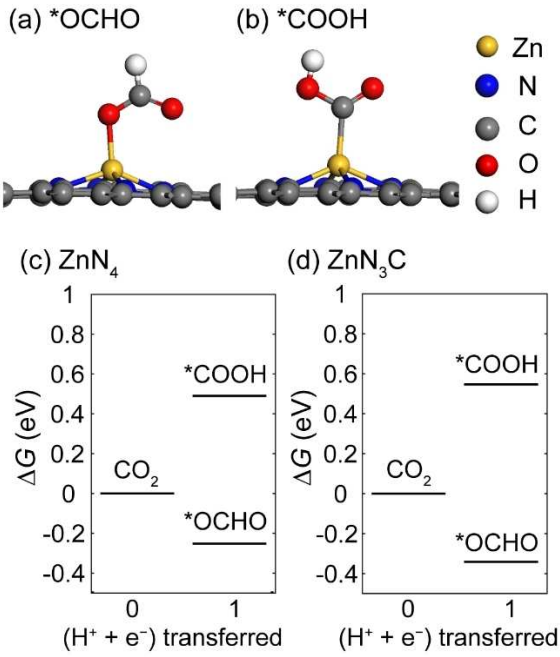

Figure 2. Atomic structures of (a) *OCHO and (b) *COOH on the Zn site in a ZnN_4 moiety. (c) and (d) are the reaction free energies of the reduction of CO_2 to *OCHO and *COOH on the Zn site in a ZnN_4 and ZnN_3C moiety at zero bias, respectively.

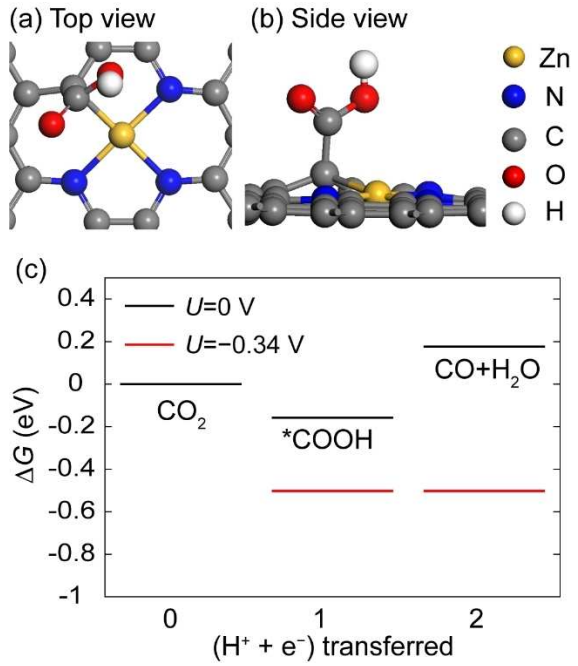

Figure 3. (a) Top and (b) side views of the atomic structure of *COOH on the C_{NN} site. (c) Free-energy diagram for the CO_2R pathway to CO on the C_{NN} site.

calculated to be 0.91 eV at zero bias. The weak binding of CO to the active site indicates facile production of CO as a gaseous species. However, the formation of *CO can become exergonic at negatively large potentials, opening the pathway to CH_4, another CO_2R product that was found below −1 V vs. RHE in experiments[19] (we present a possible electrochemical route to CH_4 in Figure S2). We find that applying a small negative potential of −0.34 V vs. RHE is enough to obtain the zero-reaction energy for $*COOH + H^+ + e^- \rightarrow * + CO + H_2O$. As a result, every successive reaction step in the pathway to CO becomes downhill in energy at this potential. This benign free-energy path to CO illustrates that the C_{NN} site can constitute crucial active sites for CO production. Moreover, from kinetic analysis using the climbing image nudged elastic band method,[29–31] we further confirm that the kinetic barriers for the reaction path in Figure 3c are small enough for CO production to occur fast at room temperature;[32] the kinetic barriers of the first and second protonation steps are less than 0.8 eV at potentials below −0.4 V vs. RHE (see details about kinetic analysis and Figures S3–S5 in the Supporting Information).

The similar reaction free energies between the *OCHO formation on the Zn site and the *COOH formation on the C_{NN} site imply that CO_2R reactions may proceed simultaneously on the Zn and C_{NN} sites of a single ZnN_3C moiety. To see effects of such concurrent CO_2R reactions on the catalytic activity of the C_{NN} atom, we examine the free-energy diagram of the CO_2R pathway to CO on the C_{NN} site, when a certain intermediate exists on the neighboring Zn site. According to the previous calculations[19] as well as the present results (Figure S6), the CO_2R reaction on the Zn site is difficult to proceed beyond the second protonation step at small negative potentials because of unfavorable energetics. Thus, we consider *OCHO and *OCHOH to be the possible intermediate on the neighboring Zn site during the concurrent CO_2R reactions. The presence of *OCHO on the neighboring Zn site is found to slightly modify the free-energy diagram in comparison to that without the *OCHO (Figure 4a); the potential limiting step that yields the largest reaction free energy is changed from the formation of CO to that of *COOH. However, we notice that the reaction energy to form *COOH is still only 0.29 eV. Accordingly, all the reaction steps become downhill in energy at −0.29 V vs. RHE. Meanwhile, *OCHOH on the neighboring Zn site rarely changes the free-energy diagram comparing to that without the *OCHOH, and we only observe a slight decrease in the reaction energy of the protonation of *COOH by 0.08 eV (Figure 4b). As a result, a downhill electrochemical route occurs at −0.26 V vs. RHE. Overall, we confirm that the simultaneous CO_2R reactions do not deteriorate the excellent catalytic activity of the C_{NN} site.

As demonstrated above, an important feature of the C_{NN} atom that enables CO production is that, unlike the single Zn atom, it allows to form *COOH rather than *OCHO. To gain insights into the favorable formation of *COOH on the C_{NN} site, we analyze a change in the electronic structure of a ZnN_3C moiety upon *COOH adsorption. In Figure 5a, we present orbital-resolved partial density of states (DOSs) of bulk carbon atoms and C_{NN} before *COOH adsorption. We pay attention to $2p_z$ states that are crucial in forming a chemical bond with the adsorbate (all of C atoms except for the C_{NN} are considered bulk atoms). For the bulk carbon atoms, we see a uniform

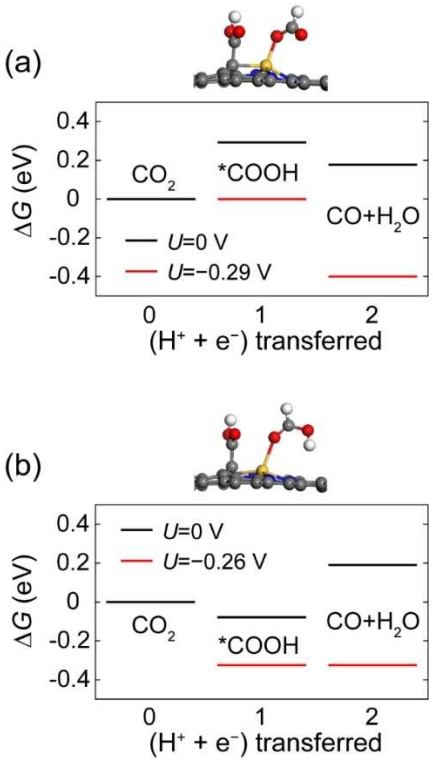

Figure 4. Free-energy diagrams for the pathways to CO on the C_{NN} site when (a) *OCHO and (b) *OCHOH are present on the neighboring Zn site.

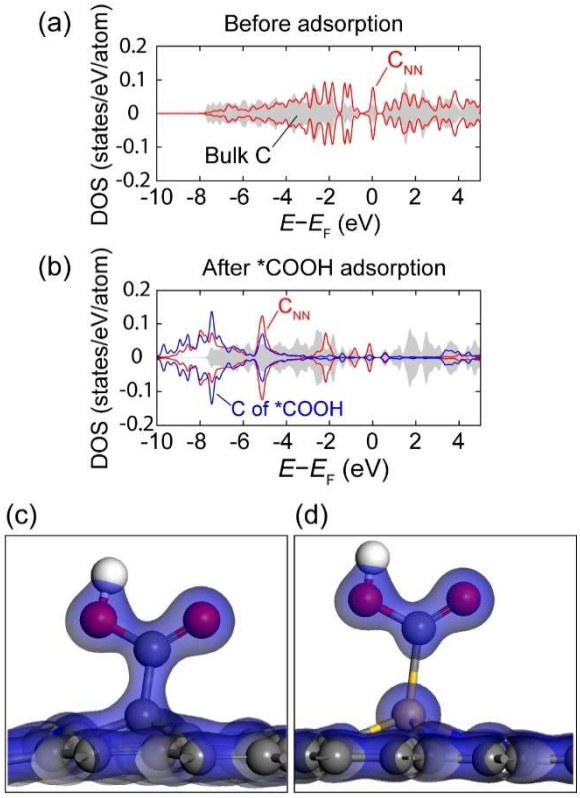

Figure 5. (a) DOSs of bulk carbon atoms and C_{NN} for $2p_z$ states in a pure ZnN_3C model. (b) DOSs of bulk carbon atoms, C_{NN}, and C of *COOH for $2p_z$ states after *COOH adsorption. Up- and down-spin DOSs are presented as + and − values, respectively, and the *x*-axis is the electron energy (*E*) with respect to the Fermi level E_F. (c) and (d) are charge density isosurfaces of *COOH adsorbed on the C_{NN} and Zn sites in a ZnN_3C moiety, respectively. Isovalues are set to 1.05 e Å^{-3} in both (c) and (d).

distribution of the DOS over a wide energy range. This is because the $2p_z$ states form continuous π bonds, giving rise to dispersive bands. Compared to the bulk carbon atoms, DOS of the C_{NN} atom is pronounced near the Fermi level. This implies that the $2p_z$ state of the C_{NN} atom is somewhat localized near the C_{NN} site. Moreover, the C_{NN} atom is almost electrically neutral (+0.24e from Bader analysis).[33] Owing to the localized $2p_z$ orbital and the neutral charge state, the C_{NN} atom can form a C–C covalent bond with C in the COOH radical that has an unsaturated dangling bond, thus lowering the electronic energies (Figure 5b). The covalent nature of the chemical bond between the C_{NN} and *COOH is also confirmed by the charge density distribution in Figure 5c. It should be noted that formation of *COOH on a bulk site is unfavorable because it disrupts the π connections extended over bulk carbon atoms. We indeed find that the reaction energy of the *COOH formation is around 2 eV larger on a bulk C site than that on the C_{NN} site. Moreover, the Zn atom in a ZnN_3C (as well as ZnN_4) moiety is positively charged due to the electron transfer from Zn to neighboring atoms (+1.2e from Bader analysis). As a result, the Zn atom is expected to form an ionic bond with adsorbates. This speculation is confirmed by the charge density analysis of the ZnN_3C moiety where *COOH is adsorbed on the Zn site (Figure 5d). Thus, considering that the O atoms in a OCHO radical have large negative partial charges, we can understand the reason why *OCHO is stable on the Zn site.

Lastly, to assess the effect of Zn doping on the CO_2R activity of the C_{NN} atom, we reexamine the free-energy diagram of the CO_2R route to CO on the C_{NN} site when the Zn atom is missing (i.e., N_3C moiety), as shown in Figure 6. We find that the reaction free energy of the *COOH formation is significantly negative (−1.08 eV). Namely, *COOH is excessively stable. Accordingly, the C_{NN} site is no longer active for CO_2R at small applied potentials; the bias required to make every reaction step exergonic increases from −0.34 V vs. RHE in a ZnN_3C moiety to −1.29 V vs. RHE in a N_3C moiety. This result is in line with experiments where N doping alone does not enhance the CO_2R activity of graphene.[16] The undesirably strong binding of COOH to the C_{NN} atom in a N_3C moiety is associated with the presence of a non-bonding state of the C_{NN} atom; besides the $2p_z$ state, the in-plane component of 2p states of the C_{NN} atom towards the divacancy site are coupled with the states of *COOH, being a source of the further reduction of the electronic energies (Figure S7). As a result of this coupling, *COOH is inclined to the divacancy site to some extent (Figure 6).

Conclusion

In summary, we investigated CO_2R pathways on Zn–N–G catalyst by using DFT calculations and the CHE model. In contrast to the widely accepted scenario that single metal atoms serve as catalytic sites, we demonstrated that the Zn atoms cannot be the active sites yielding CO as a CO_2R product because of the formation of *OCHO at the initial protonation step. As an alternative, we suggested the C_{NN} site in a ZnN_3C moiety, and the CO_2R route to CO on the C_{NN} site was found to be energetically benign. In addition, we revealed that Zn doping is critical for the C_{NN} atom to exhibit high CO_2R activity. By identifying the active site for CO_2R in the Zn–N–G catalyst, we believe that this work will help design advanced graphene-based single-atom catalysts.

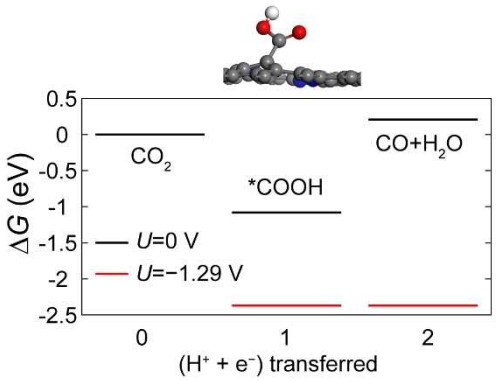

Figure 6. Free-energy diagram of the pathway to CO on the C_{NN} site in a N_3C moiety.

Experimental Section

Our DFT calculations are performed by using the Vienna ab initio simulation package (VASP) with the PAW pseudopotentials.[34,35] We employ the revised PBE (RPBE) exchange-correlation functional that is known to accurately describe molecular adsorption energies.[2,36,37] An atomic model of the Zn–N–G catalyst is constructed using a 6× 6 graphene supercell. To avoid the interaction between periodic images along the vertical direction, we insert a vacuum with thickness of around 10 Å into the supercell. The energy cutoff for the plane-wave basis is set to 400 eV and a 3×3×1 Γ-centered *k*-point mesh is used for the Brillouin-zone sampling. The van der Waals interactions are considered by using DFT-D3 Grimme method.[38] Solvation effects are taken into account by the implicit solvation model that treats the water environment as the continuum dielectric medium. This method is computationally efficient and fast, and was successfully applied to investigating electrochemical reactions in previous works.[39,40] We confirmed that the implicit model yields a solvation energy of an adsorbate comparable to the one obtained using the explicit model in which the water environment is modelled by including a few water molecules in a supercell; we calculated the solvation energy of *COOH to be 0.25 eV (i.e., *COOH is further stabilized in the water environment) which is consistent with 0.25 eV for *R-OH in previous studies using the explicit solvation model.[2,41] Throughout our calculations, spin-polarization is included. All atomic configurations are relaxed until atomic forces become less than 0.05 eV $Å^{-1}$.

The reaction free energy associated with the proton-coupled electron transfer reduction is calculated based on the widely-used computational hydrogen electrode model.[2] In the CHE model, the free energy of a proton-electron pair at 0 V vs. RHE is set to half of the free energy of gaseous hydrogen at 1 atm, namely $G(H^+)+G(e^-)=\frac{1}{2}G(H_2$ at 1 atm), by definition of RHE. The effect of the external potential (U) with respect to RHE on the reaction free energy is considered by shifting the free energy of the electron by $-eU$, where e is the magnitude of the electron charge. Herein, to obtain free energies of adsorbates, we add the zero-point energy (ZPE) and vibrational entropy at the room temperature, which are computed within the harmonic approximation, to the DFT energy of adsorbates. For calculating free energies of gas species, we evaluate ZPEs based on calculated vibrational frequencies, whereas experimental entropies are taken from the NIST webbook.[42] The free energy of a H_2O molecule in aqueous medium is obtained as that of gaseous H_2O assuming that water is in equilibrium with its vapor at a partial pressure of 0.035 atm, following a previous work.[2] RPBE energies of gas-phase molecules with the OCO backbone are known to include a systematic error. To correct this, we add 0.45 eV to the DFT energy of the CO_2 molecule.[2] All the free-energy components (i.e., ZPE, entropy, and DFT energy) considered in the present work are provided in the Supporting Information.

Acknowledgements

This work was supported by the Creative Materials Discovery Program through the National Research Foundation of Korea (NRF) funded by the Ministry of Science and ICT (2017 M3D1 A1040688).

Conflict of Interest

The authors declare no conflict of interest.

Keywords: CO_2 reduction · density functional calculations · graphene · single-atom catalysts · zinc

[1] W. Zhu, R. Michalsky, Ö. Metin, H. Lv, S. Guo, C. J. Wright, X. Sun, A. A. Peterson, S. Sun, *J. Am. Chem. Soc.* **2013**, *135*, 16833.
[2] A. A. Peterson, F. Abild-Pedersen, F. Studt, J. Rossmeisl, J. K. Nørskov, *Energy Environ. Sci.* **2010**, *3*, 1311.
[3] Y. Hori, A. Murata, R. Takahashi, *J. Chem. Soc. Faraday Trans. 1* **1989**, *85*, 2309.
[4] D. H. Won, H. Shin, J. Koh, J. Chung, H. S. Lee, H. Kim, S. I. Woo, *Angew. Chem. Int. Ed.* **2016**, *55*, 9297; *Angew. Chem.* **2016**, *128*, 9443.
[5] M. Li, S. Garg, X. Chang, L. Ge, L. Li, M. Konarova, T. E. Rufford, V. Rudolph, G. Wang, *Small Methods* **2020**, *4*, 2000033.
[6] N. Hoshi, M. Noma, T. Suzuki, Y. Hori, *J. Electroanal. Chem.* **1997**, *421*, 15.
[7] C. Costentin, M. Robert, J.-M. Savéant, *Chem. Soc. Rev.* **2013**, *42*, 2423.
[8] Y. Li, Q. Sun, *Adv. Energy Mater.* **2016**, *6*, 1600463.
[9] S. Kang, S. Han, Y. Kang, *ChemSusChem* **2019**, *12*, 2671.
[10] S. Kang, S. Ju, S. Han, Y. Kang, *J. Phys. Chem. C* **2020**, *124*, 25812.
[11] S. A. Francis, J. M. Velazquez, I. M. Ferrer, D. A. Torelli, D. Guevarra, M. T. McDowell, K. Sun, X. Zhou, F. H. Saadi, J. John, *Chem. Mater.* **2018**, *30*, 4902.
[12] K. U. D. Calvinho, A. B. Laursen, K. M. K. Yap, T. A. Goetjen, S. Hwang, N. Murali, B. Mejia-Sosa, A. Lubarski, K. M. Teeluck, E. S. Hall, *Energy Environ. Sci.* **2018**, *11*, 2550.
[13] X. Qin, S. Zhu, F. Xiao, L. Zhang, M. Shao, *ACS Energy Lett.* **2019**, *4*, 1778.
[14] X. Zu, X. Li, W. Liu, Y. Sun, J. Xu, T. Yao, W. Yan, S. Gao, C. Wang, S. Wei, Y. Xie, *Adv. Mater.* **2019**, *31*, 1808135.
[15] A. S. Varela, N. Ranjbar Sahraie, J. Steinberg, W. Ju, H. S. Oh, P. Strasser, *Angew. Chem. Int. Ed.* **2015**, *54*, 10758; *Angew. Chem.* **2015**, *127*, 10908.
[16] F. Yang, P. Song, X. Liu, B. Mei, W. Xing, Z. Jiang, L. Gu, W. Xu, *Angew. Chem. Int. Ed.* **2018**, *57*, 12303; *Angew. Chem.* **2018**, *130*, 12483.
[17] Z. Zhang, J. Xiao, X. J. Chen, S. Yu, L. Yu, R. Si, Y. Wang, S. Wang, X. Meng, Y. Wang, Z. Q. Tian, D. Deng, *Angew. Chem. Int. Ed.* **2018**, *57*, 16339; *Angew. Chem.* **2018**, *130*, 16577.
[18] Z. Chen, K. Mou, S. Yao, L. Liu, *ChemSusChem* **2018**, *11*, 2944.
[19] L. Han, S. Song, M. Liu, S. Yao, Z. Liang, H. Cheng, Z. Ren, W. Liu, R. Lin, G. Qi, X. Liu, Q. Wu, J. Luo, H. L. Xin, X. Liu, Q. Wu, J. Luo, H. L. Xin, *J. Am. Chem. Soc.* **2020**, *142*, 12563.
[20] W. Ju, A. Bagger, G. P. Hao, A. S. Varela, I. Sinev, V. Bon, B. Roldan Cuenya, S. Kaskel, J. Rossmeisl, P. Strasser, *Nat. Commun.* **2017**, *8*, 944.
[21] H. Bin Yang, S. F. Hung, S. Liu, K. Yuan, S. Miao, L. Zhang, X. Huang, H. Y. Wang, W. Cai, R. Chen, J. Gao, X. Yang, W. Chen, Y. Huang, H. M. Chen, C. M. Li, T. Zhang, B. Liu, *Nat. Energy* **2018**, *3*, 140.
[22] H. Bao, Y. Qiu, X. Peng, J. Wang, Y. Mi, S. Zhao, X. Liu, Y. Liu, R. Cao, L. Zhuo, J. Ren, J. Sun, J. Luo, X. Sun, *Nat. Commun.* **2021**, *12*, 238.
[23] L. Han, Z. Ren, P. Ou, H. Cheng, N. Rui, L. Lin, X. Liu, L. Zhuo, J. Song, J. Sun, J. Luo, H. L. Xin, *Angew. Chem. Int. Ed.* **2021**, *60*, 345; *Angew. Chem.* **2021**, *133*, 349.
[24] L. Han, M. Hou, P. Ou, H. Cheng, Z. Ren, Z. Liang, J. A. Boscoboinik, A. Hunt, I. Waluyo, S. Zhang, L. Zhuo, J. Song, X. Liu, J. Luo, H. L. Xin, *ACS Catal.* **2021**, *11*, 509.
[25] J. Xu, S. Lai, D. Qi, M. Hu, X. Peng, Y. Liu, W. Liu, G. Hu, H. Xu, F. Li, C. Li, J. He, L. Zhuo, J. Sun, Y. Qiu, S. Zhang, J. Luo, X. Liu, *Nano Res.* **2021**, *14*, 1374.
[26] K. Jiang, S. Siahrostami, T. Zheng, Y. Hu, S. Hwang, E. Stavitski, Y. Peng, J. Dynes, M. Gangisetty, D. Su, K. Attenkofer, H. Wang, *Energy Environ. Sci.* **2018**, *11*, 893.
[27] T. Kropp, M. Mavrikakis, *ACS Catal.* **2019**, *9*, 6864.
[28] S. Kabir, K. Artyushkova, A. Serov, B. Kiefer, P. Atanassov, *Surf. Interface Anal.* **2016**, *48*, 293.
[29] G. Henkelman, B. P. Uberuaga, H. Jónsson, *J. Chem. Phys.* **2000**, *113*, 9901.
[30] S. A. Akhade, N. J. Bernstein, M. R. Esopi, M. J. Regula, M. J. Janik, *Catal. Today* **2017**, *288*, 63.
[31] W. Luo, X. Nie, M. J. Janik, A. Asthagiri, *ACS Catal.* **2016**, *6*, 219.
[32] J. H. Montoya, C. Shi, K. Chan, J. K. Nørskov, *J. Phys. Chem. Lett.* **2015**, *6*, 2032.
[33] W. Tang, E. Sanville, G. Henkelman, *J. Phys. Condens. Matter* **2009**, *21*, 84204.
[34] G. Kresse, J. Furthmüller, *Phys. Rev. B* **1996**, *54*, 11169.
[35] G. Kresse, D. Joubert, *Phys. Rev. B* **1999**, *59*, 1758.
[36] B. Hammer, L. B. Hansen, J. K. Nørskov, *Phys. Rev. B* **1999**, *59*, 7413.

[37] J. Wellendorff, K. T. Lundgaard, A. Møgelhøj, V. Petzold, D. D. Landis, J. K. Nørskov, T. Bligaard, K. W. Jacobsen, *Phys. Rev. B* **2012**, *85*, 235149.
[38] S. Grimme, J. Antony, S. Ehrlich, H. Krieg, *J. Chem. Phys.* **2010**, *132*, 154104.
[39] Y. Sha, T. H. Yu, Y. Liu, B. V. Merinov, W. A. Goddard III, *J. Phys. Chem. Lett.* **2010**, *1*, 856.
[40] K. Mathew, R. Sundararaman, K. Letchworth-Weaver, T. A. Arias, R. G. Hennig, *J. Chem. Phys.* **2014**, *140*, 84106.
[41] V. Tripkovic, E. Skulason, S. Siahrostami, J. K. Nørskov, J. Rossmeisl, *Electrochim. Acta.* **2010**, *55*, 7975.
[42] W. G. Mallard, P. J. Linstrom, *Natl. Inst. Stand. Technol. Gaithersbg. MD* **2011**, 20899.

Manuscript received: April 13, 2021
Revised manuscript received: April 20, 2021
Accepted manuscript online: April 21, 2021
Version of record online: May 7, 2021